

Rose-Petal-Like Morphology of Yttrium Molybdate Nanosheets (YMoO₄) Anchored on Functionalized Carbon Nanofibers: An Efficient Electrocatalyst for the Electrochemical Sensing of bisphenol-A

Ramachandran Rajakumaran¹, Settu Ramki¹, Shen-Ming Chen^{1,*}, Tse-Wei Chen^{2,3}, Selvakumar Veerasankar⁴, Tien-Wen Tseng^{2,*}, Chih-Ching Huang^{5,*}

¹ Electroanalysis and Bioelectrochemistry Lab, Department of Chemical Engineering and Biotechnology, National Taipei University of Technology, Taipei 10608, Taiwan

² Department of Chemical Engineering and Biotechnology, National Taipei University of Technology, Taipei 10608, Taiwan

³ Research and Development Center for Smart Textile Technology, National Taipei University of Technology, Taipei 106, Taiwan, ROC.

⁴ Integrated Technology Complex Department of Energy and Refrigeration Air-conditioning Engineering, National Taipei University of Technology, Taipei 10608, Taiwan

⁵ Department of Bioscience and Biotechnology, National Taiwan Ocean University, 2, Beining Road, Keelung 20224, Taiwan

*E-mail: smchen78@ms15.hinet.net (Shen-Ming Chen), f10403@ntut.edu.tw (Tien-Wen Tseng), huangcing@ntou.edu.tw (Chih-Ching Huang)

Received: 18 February 2019 / Accepted: 22 April 2019 / Published: 10 June 2019

The current study aims to develop the electrochemical sensor based on the rarely studied metal molybdate. Based on this view, we have developed a novel yttrium molybdate (YMoO₄) nanosheets (NSs) using wet-chemical method. Further, the conductivity of YMoO₄ NSs was improved by integration with functionalized carbon nanofiber (f-CNF) through a simple ultrasonication method. As-prepared YMoO₄ and YMoO₄/f-CNF composite was systematically characterized by various spectroscopic techniques including XRD, RAMAN, and HR-TEM analysis. From the analysis, the successful integration of YMoO₄ with f-CNF was scrutinized. In addition, the electrocatalytic behavior of YMoO₄/f-CNF nanocomposite was investigated by the electrochemical detection of bisphenol-A (BPA) using cyclic voltammetry and differential pulse voltammetry techniques. As we expected, YMoO₄/f-CNF modified glassy carbon electrode (GCE) achieved a low detection limit of 0.01 μM and linear response range of 0.1 - 1318 μM towards the detection of BPA. From the above results clearly, evidenced that the YMoO₄/f-CNF nanocomposite was an efficient electrode material for the determination of BPA in real sample analysis.

Keywords: Metal molybdate, Nanosheets, Yttrium molybdate, Functionalized carbon nanofiber, Electrochemical sensor, Bisphenol-A.

1. INTRODUCTION

Bisphenol A (2,2-bis (4-hydroxy phenyl) propane, BPA) is one the most important organic monomer mainly used for the synthesis and fabrication of epoxy resin [1]. In addition, this phenolic resin which is commercially used for the production of polycarbonate plastics due to its wide application in manufacturing of products like infant milk bottles [2, 3], reusable plastic food container [4], nursing bottle [5], beverage packaging, medical devices [6] and food cans coating [7]. BPA is one of the major endocrine disrupting compounds and it can able to mimic the natural hormone by occupying the estrogen binding receptor and disturbs the natural metabolic function of hormones [8]. Besides, BPA is a lipophilic compound and used for the packing of food materials which leads to the cause of harmful effect to the human such as less reproductivity of sperms [9]. Further, it may lead to cause of infertility, diabetes, and obesity [10-13]. Additionally, the higher intake of BPA in human system can induces some risk factors such as cardiovascular disease, breast cancer, prostate cancer, pleiotropic problems in brain [14], neural changes in children [15], and liver damage [16]. As an endocrine disrupter in humans, it may cause some adverse effects which includes lowering of immune response even at low level and primarily it affects endogenous hormones of estrogen and androgen [17, 18]. Moreover, BPA stops the metabolic function of thyroid hormone [19]. Furthermore, it is enormously distributed and continuously leached into the aquatic environment by releasing the waste sewage effluent from plastic manufacturing industries directly into the rivers may adversely affect the water resources and wildlife animals [20-22]. It also stimulates acute toxic effects in marine species like fish, reptiles by causing feminization and seriously produces tremendous problems in affecting their growth and development of living organisms in the ecosystem [23-25]. Therefore, it is most important concern to detect BPA level to avoid harmful threatening of human system and environmental factors. For that, various techniques have been developed namely Raman scattering (SERS), gas chromatography with mass spectrometry, fluorescence [26], chemiluminescence [27], liquid chromatography combined with mass spectrometry solid phase micro extraction, piezoelectric bio-sensing [28], enzyme-linked immunosorbent assay (ELISA) [29], and capillary electrophoresis [30]. Although, these techniques are highly expensive, complex to process, more time consuming and exhibits poor selectivity [31]. Therefore, in order to overcome such issues, electrochemical sensor is applied for the detection of BPA due to its low cost, less time to operate, high selectivity and high sensitivity [32-34].

Until now, various nanomaterials such as carbon materials, conductive polymers, metal oxides, and metal sulfides has been applied for the detection of BPA. Among them, metal molybdates are consider as a more efficient electrocatalyst due to their unique properties, especially, high electrocatalytic activity [35, 36]. Moreover, the metal molybdate are considered as an important class of inorganic materials and applied for various application such as catalysis, electronics and optoelectronics due to their large surface area, and high reactive sites [37, 38]. Furthermore, metal molybdate is exist in two different forms such as scheelite and wolframite structure which is based on the valency of the binding metal atom [35]. While, mono or bivalent atom is coordinate with molybdenum through either

distorted phase of tetrahedral or octahedral coordination sites [39]. Generally, metal molybdate exhibits large surface area, high electrical conductivity, and cyclic stability when compared to other metal oxides [38]. Additionally, molybdate can exist in different oxidation states (Mo^{4+} & Mo^{6+}) with a higher storage capacity and energy density [40]. Further, the combination of molybdate with transition or other rare-earth metal will be shows enhanced electrocatalytic activity due to the higher basicity, large surface area and chemical stability. Among the metal molybdates, yttrium (Y) based molybdate is considered as most suitable for the electrochemical sensing application because of their larger ionic radius (0.91 Å) and higher surface basicity [41]. More evidently, Chen et al., designed a novel yttrium molybdate based electrocatalyst for effective detection and degradation of acebutolol [42,]. Similarly, C. Li et al., introduced metal organic framework/graphene based electrochemical sensing electrode material for the sensing of BPA [43]. Therefore, it is concluded that the YMoO_4 is a more selective electrocatalyst for the electrochemical sensing application. Furthermore, the electrocatalytic activity of YMoO_4 was improved by the combination of carbon nanomaterials.

Different carbon nanomaterials such as graphene oxide, carbon nanotube, carbon nano horn, and carbon nanofiber are widely used for the electrochemical sensing applications [44-47]. Among them, carbon nanofiber (CNF) act as a more suitable electrode material for electrochemical application because of their wide potential window, low cost and chemical inertness in various electrolyte solution. [48]. The structure of CNF is composed of different stacking arrangement of graphene sheets such as stacked platelet or herringbone structure. Generally, the pristine CNF exhibits less solubility and electrical conductivity. While, the functionalization of CNF by acid treatment will improve its solubility and electrical conductivity due to the introduction of large number of functional groups on its open-end structure. Further, functionalization of CNF will impart large number of edge plane defective sites for efficient electron transport [49]. Therefore, it is confirmed that the integration of f-CNF with YMoO_4 ($\text{YMoO}_4/\text{f-CNF}$) will effectively enhanced the property of electrochemical sensing behavior of BPA through imparting high ion diffusion pathway.

In this work, we have synthesized $\text{YMoO}_4/\text{f-CNF}$ nanocomposite by a simple sonochemical method. As-prepared $\text{YMoO}_4/\text{f-CNF}$ nanocomposite was characterized by using various spectroscopic techniques such as XRD, RAMAN, and HR-TEM analysis. All the characterization techniques result confirmed that the formation of $\text{YMoO}_4/\text{f-CNF}$ nanocomposite through ultrasonication method and applied for the electrochemical detection of BPA. For that, electrochemical sensing behavior of $\text{YMoO}_4/\text{f-CNF}$ nanocomposite was studied by cyclic voltammetry (CV) and differential pulse voltammetry (DPV) techniques. Remarkably, the proposed $\text{YMoO}_4/\text{f-CNF}$ nanocomposite sensor exhibits excellent electrocatalytic activity towards the detection of BPA.

2. EXPERIMENT SECTION

2.1 Materials and reagents

The yttrium nitrate hexahydrate ($\text{Y}(\text{NO}_3)_3 \cdot 6\text{H}_2\text{O}$), sodium molybdate dihydrate ($\text{Na}_2\text{MoO}_4 \cdot 2\text{H}_2\text{O}$), urea ($\text{CH}_4\text{N}_2\text{O}$), and bisphenol A ($\text{C}_{15}\text{H}_{16}\text{O}_2$) were purchased from Sigma-Aldrich

chemical Company & Co. Ltd. The phosphate buffer (pH 7, 0.05 M) solution used as a supporting electrolyte for the entire electrochemical measurements towards BPA sensing.

2.2. Synthesis of rose petal-like YMoO_4 and $\text{YMoO}_4/\text{f-CNF}$ nanocomposite

The YMoO_4 nanosheets was prepared by following our previous synthesis method [42]. In the typical synthesis, about 0.1 M of $(\text{Y}(\text{NO}_3)_3 \cdot 6\text{H}_2\text{O})$, and 0.2 M of $\text{Na}_2\text{MoO}_4 \cdot 2\text{H}_2\text{O}$ were mixed together in a 70 mL double distilled water (DD) under constant stirring. Afterward, 1 M of urea (0.6 g in 10 mL DD) was added to the above solution and allowed to constant stirring for 1 hr. Subsequently, the obtained white colored precipitate was filtered off and washed with DD water by several times using ethanol and centrifugation. After drying, the products were annealed under the air atmosphere at 650 °C for 4 hr. Finally, the calcined product was used for the nanocomposite preparation. The functionalization of carbon nanofiber (f-CNF) was prepared by following our previous reported article [47]. For $\text{YMoO}_4/\text{f-CNF}$ nanocomposite preparation, 100 mg of YMoO_4 and 40 mg of f-CNF were dispersed in 100 mL DD and ultrasonicated for 60 min. Finally, the prepared product obtained combination of two nanomaterial was dried at ambient temperature and denoted as $\text{YMoO}_4/\text{f-CNF}$ s nanocomposite.

2.3. Characterization techniques

The crystalline nature and lattice parameter of as-prepared YMoO_4 and $\text{YMoO}_4/\text{f-CNF}$ were investigated using X-ray diffraction technique (XRD, XPERT-3 diffractometer with Cu $K\alpha$ radiation ($K= 1.54 \text{ \AA}$)). Additionally, the surface morphology of the YMoO_4 and $\text{YMoO}_4/\text{f-CNF}$ nanocomposite was studied using high resolution transmission electron microscopy (HR-TEM: JEOL 2100F) analysis. The structural finger print of the prepared samples were reported using Raman spectroscopy (WITech CRM200 confocal microscopy, Raman system with a 488 nm laser). Consequently, the electrochemical performance of different modified electrodes towards the sensing of BPA were studied by using CV and DPV techniques (CHI 405a and CHI 900 Electrochemical analyzer, made in USA). All followed electrochemical studies were performed at room temperature. The electrochemical properties of the prepared samples were carried out by conventional three electrode systems, whereas, the glassy carbon electrode (GCE, working area = 0.07 cm^2) was used as a working electrode, platinum (Pt) wire was used as a counter electrode, and Ag/AgCl (KCl.sat) was used as a reference electrode.

2.4. Fabrication of $\text{YMoO}_4/\text{f-CNF}/\text{GCE}$

For the fabrication process, 2 mg of $\text{YMoO}_4/\text{f-CNF}$ nanocomposite was redispersed in 1 mL of DD water and allowed to ultrasonication for 15 min. Then, the dispersed $\text{YMoO}_4/\text{f-CNF}$ (8 μL) was coated on the polished surface of GCE and kept at ambient temperature for 15 min. After drying, the fabricated of $\text{YMoO}_4/\text{f-CNF}$ modified electrode was rinsed with DD water to remove the un-bounded materials on the surface of GCE. Finally, the $\text{YMoO}_4/\text{f-CNF}/\text{GCE}$ was used as an operational electrode in all electrochemical experiment. For the comparison process, the other modified electrodes such as YMoO_4/GCE and f-CNF/GCE were fabricated by following the same procedures.

3. RESULTS AND DISCUSSION

3.1 Characterization of YMoO_4 and $\text{YMoO}_4/\text{f-CNF}$ nanocomposite

The lattice parameter and crystalline nature of YMoO_4 and $\text{YMoO}_4/\text{f-CNF}$ nanocomposite was studied by XRD technique. Figure 1A,B shows the XRD pattern of YMoO_4 and $\text{YMoO}_4/\text{f-CNF}$ nanocomposite. From the Figure 1A, it is clear that the diffraction peaks of YMoO_4 are appears at the diffraction angle of $2\theta = 29.4^\circ, 32.5^\circ, 34.7^\circ, 39.9^\circ, 48.3^\circ, 49.9^\circ, 56.1^\circ, 58.9^\circ, 60.8^\circ, 73.2^\circ,$ and 78.4° corresponding to the (112), (004), (200), (211), (204), (220), (116), (312), (224), (400), and (316) planes of tetragonal YMoO_4 , respectively, with the space group of $I4_1/a$ (88) [JCPDS no. 35-1470]. The obtained peak results are well matched with previously reported article [42]. From Figure 1B, the little broad intense peak at $2\theta = 25.7^\circ$ was observed after composite with f-CNF, which is associated to the (002) plane of f-CNF. Figure 1B clearly displayed the appearance of both YMoO_4 and f-CNF diffraction peaks in nanocomposite without any other impurities, it describes the successful preparation of nanocomposite ($\text{YMoO}_4/\text{f-CNF}$).

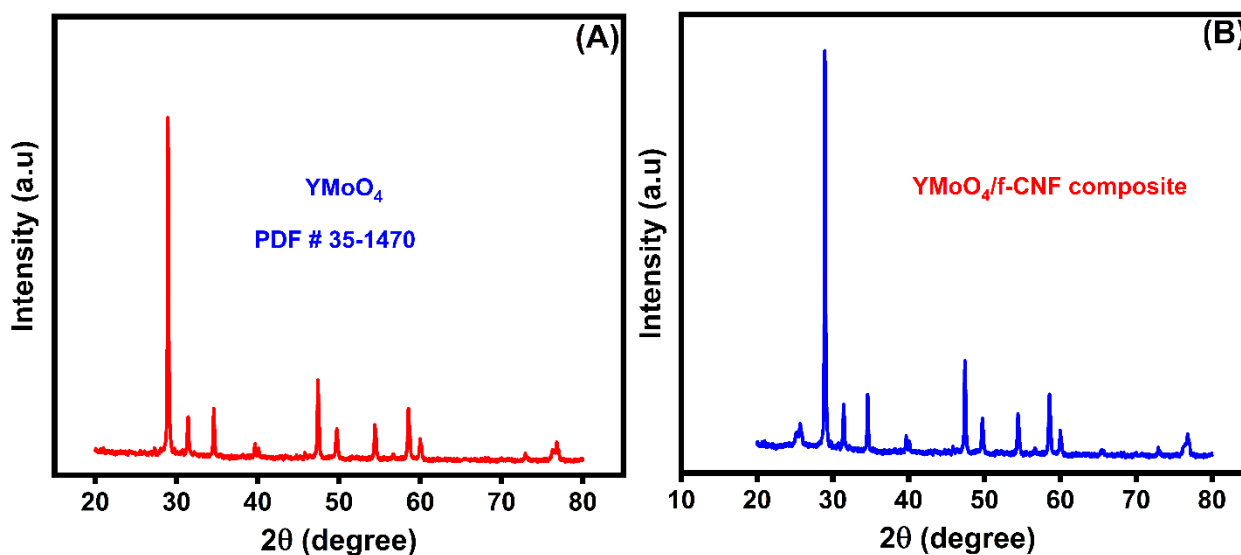


Figure 1. XRD patterns of YMoO_4 (A) and $\text{YMoO}_4/\text{f-CNF}$ (B) nanocomposite.

Additionally, the Raman spectra of YMoO_4 and $\text{YMoO}_4/\text{f-CNF}$ composites were shown in Figure 2A,B, which confirms the presence of defective surface. The Raman spectrum of YMoO_4 in Figure 2A, indicates the presence of high intensity peak at 953 cm^{-1} which is corresponds to the symmetric stretching vibration mode of MoO_4 . Besides, some peaks are observed at an intensity of 251, 365, and 445 cm^{-1} were assigned to the $\nu_2(\text{Ag})$, $\nu_4(\text{Bg})$ and $\nu_4(\text{Eg})$ bending vibration modes of Mo-O group, respectively. Figure 2B indicates the Raman spectra of $\text{YMoO}_4/\text{f-CNF}$ shows D and G band corresponding to the intensity of 1368 and 1617 cm^{-1} . In general, D band is corresponding to the disorder nature of sp^2 bonding site of graphitic carbon and G band is C-C stretching in graphitic carbon. The existence of strong peaks of YMoO_4 and f-CNF confirmed the successful formation of $\text{YMoO}_4/\text{f-CNF}$ composite. Furthermore, the morphological structure and size of as-prepared YMoO_4 , and $\text{YMoO}_4/\text{f-CNF}$

CNF composite were clearly observed by HR-TEM analysis. The Figure 3 shows the HR-TEM images of YMoO_4 , and $\text{YMoO}_4/\text{f-CNF}$ nanocomposite. From the Figure 3A,B, it can be clearly seen that the YMoO_4 are in the form of nanosheets with a thickness of 60-80 nm. Moreover, the lattice fringes with an interplanar distance of 0.303 nm corresponds to a plane of (112) indicates the formation of tetragonal phase of YMoO_4 (Figure 3C). In addition, the morphology of $\text{YMoO}_4/\text{f-CNF}$ were clearly demonstrated in Figure 3D,E, which confirms the nanosheets-like YMoO_4 decorated on the f-CNF surface. Similarly, the surface distortion of f-CNF due to the integration of YMoO_4 was clearly showed in lattice fringes as shown in Figure 3F. Interestingly, all the above studies confirmed the formation of YMoO_4 nanosheets and $\text{YMoO}_4/\text{f-CNF}$ nanocomposite.

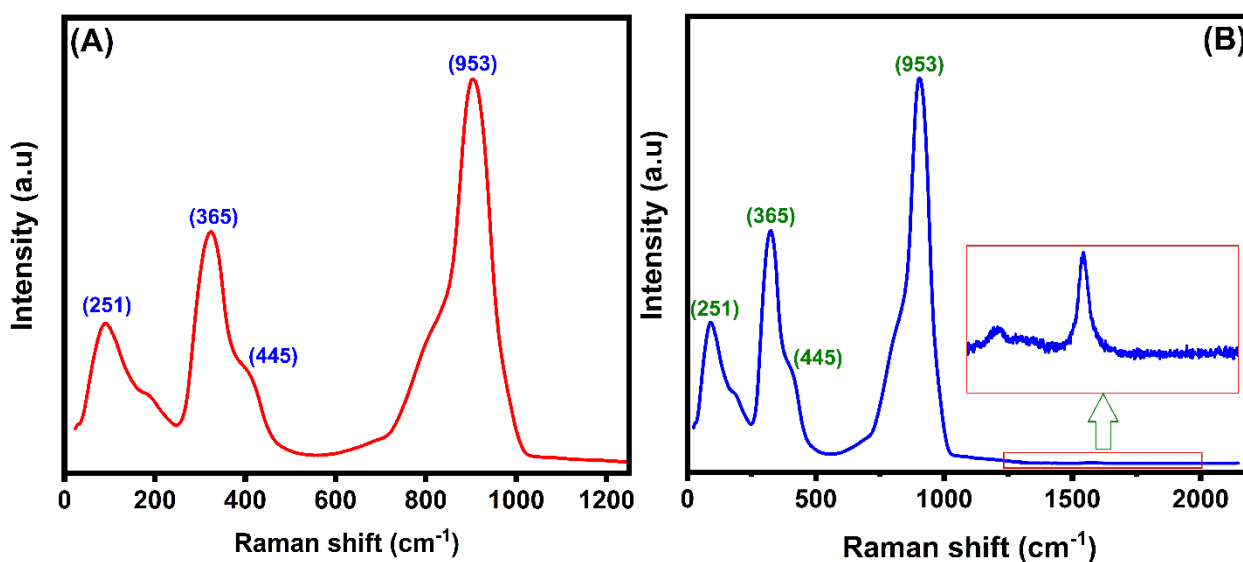


Figure 2. Raman spectra of YMoO_4 (A) and $\text{YMoO}_4/\text{f-CNF}$ (B) nanocomposite

3.2. Electrochemical determination of BPA at different modified electrodes

The electrochemical behavior of various modified electrode was studied by CV analysis. The experiment was carried out in presence of 300 μM BPA at different modified electrodes such as bare GCE (a), YMoO_4/GCE (b), f-CNF/GCE (c) and $\text{YMoO}_4/\text{f-CNF}/\text{GCE}$ (d) in N_2 saturated 0.05 PBS (pH 7) at a scan rate of 50 mVs^{-1} . The experiment was performed in the absence (a-d, Figure 4A) and presence (e-h, Figure 4B) of 300 μM BPA. In absence of BPA (Figure 4A), there is no oxidation peak was observed at all the modified and unmodified electrodes. The resultant CV curve is shown in Figure 4B(e), clearly indicates that the bare GCE exhibits less electrochemical oxidation peak response and longer peak potential when compared to YMoO_4/GCE (f), f-CNF/GCE (g) and $\text{YMoO}_4/\text{f-CNF}$ (h) modified electrodes. Whereas, the YMoO_4/GCE (f) and f-CNF/GCE (g) shows a lower oxidation peak current response for the addition of 300 μM BPA. While, there is a sharp and well-defined oxidation peak was observed in the presence of 300 μM BPA for the $\text{YMoO}_4/\text{f-CNF}/\text{GCE}$ at a low potential of 0.54 V. Moreover, the obtained oxidation peak current of BPA at $\text{YMoO}_4/\text{f-CNF}/\text{GCE}$ (103.8 μA) is higher than that of other modified electrodes such as bare GCE (0.47 μA), YMoO_4/GCE (5.01 μA) and f-CNF/GCE

(57.3 μA). The obtained result clearly suggests that the higher electrocatalytic activity of $\text{YMoO}_4/\text{f-CNF}$ composite is due to the strong interaction of BPA with f-CNF and more active sites of the YMoO_4 nanosheets, and it could provide an excellent electrochemical sensing platform for BPA detection.

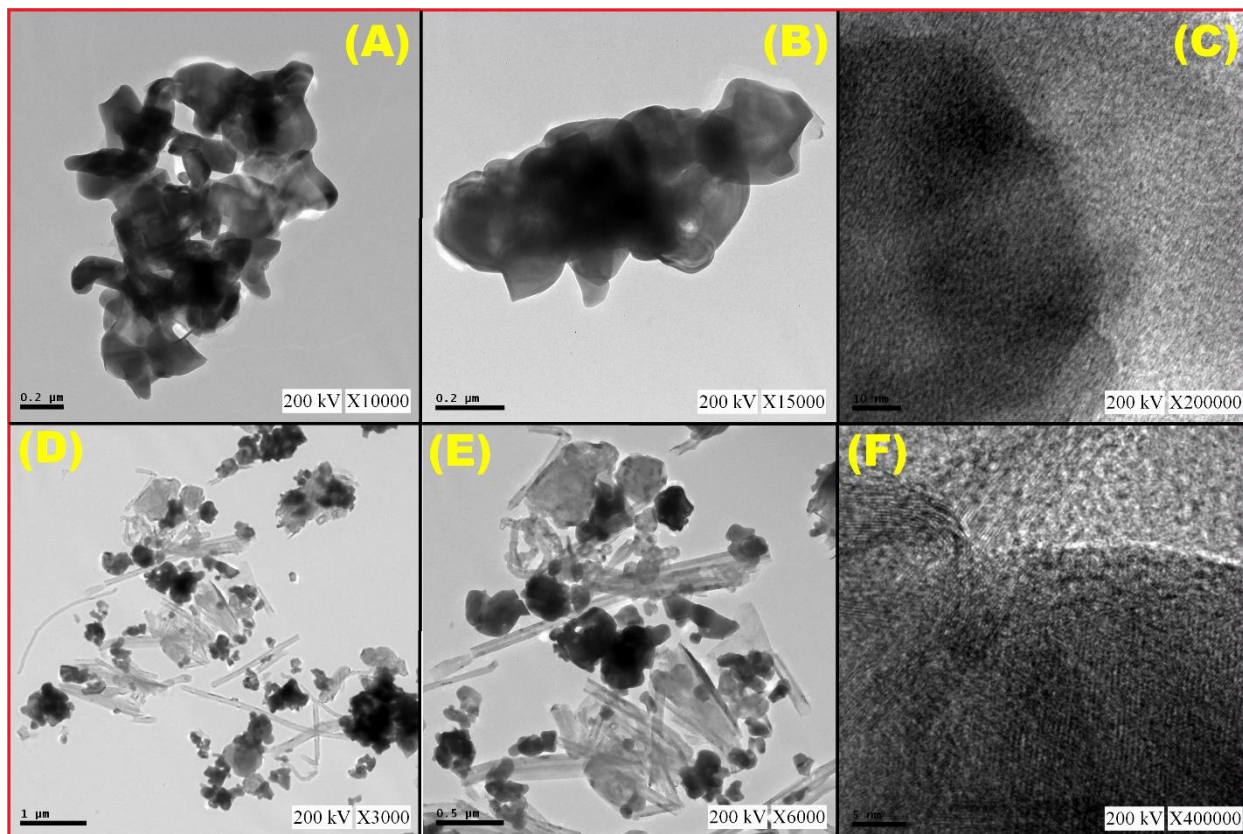


Figure 3. HR-TEM images of YMoO_4 (A-C) and $\text{YMoO}_4/\text{f-CNF}$ (D-F) nanocomposite

Generally, the oxidation of any phenolic compound at any modified electrode which leads to the formation of reduction of oxidation rate which was attributed to the formation of polymeric product. Whereas, the direct oxidation of any phenolic compound leads to the formation of phenoxy free radicals assumed as either in the form of dimeric molecules initiated by the C–O, C–C and/or O–O coupling. By following the reverse scan, there is no appearance of reduction peak was observed due to the irreversible reaction. The absence of reduction peak is due to the relative adsorption of BPA on the electrode surface. Moreover, the possible electro-oxidation mechanism of BPA on the $\text{YMoO}_4/\text{f-CNF}$ composite modified electrode is illustrated in Scheme 1.

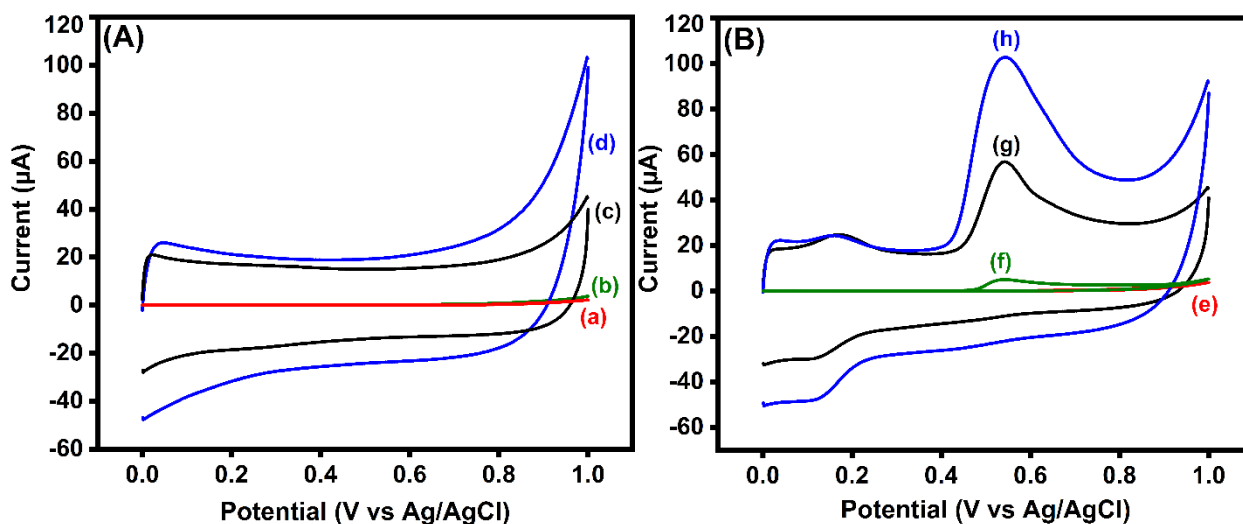
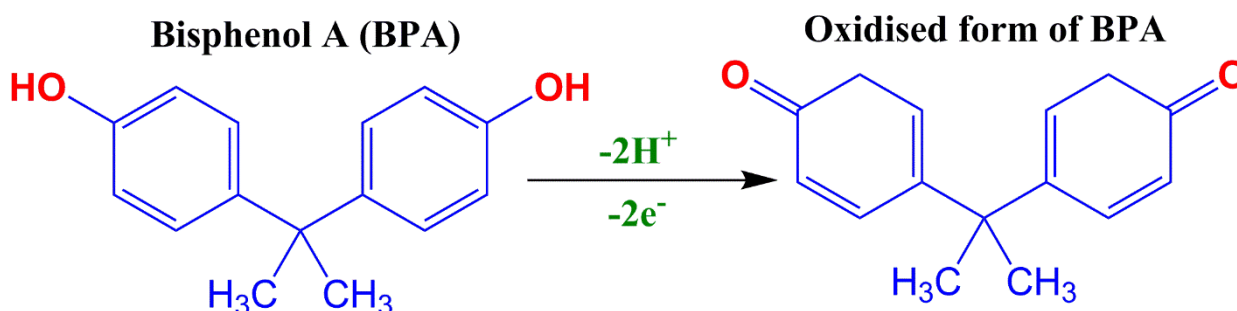


Figure 4. CVs of (a) bare GCE, (b) YMoO_4/GCE , (c) $\text{f-CNF}/\text{GCE}$ and (d) $\text{YMoO}_4/\text{f-CNF}/\text{GCE}$ in the absence (A) and presence of $300 \mu\text{M}$ BPA containing 0.05 M PBS (pH 7) at a scan rate of 50 mVs^{-1} (B).



Scheme 1. Oxidation reaction mechanism of BPA at the $\text{YMoO}_4/\text{f-CNF}$ modified electrode

3.3. Effect of concentration on $\text{YMoO}_4/\text{f-CNF}$ modified electrode

The electrocatalytic activity of $\text{YMoO}_4/\text{f-CNF}/\text{GCE}$ was investigated by varying the concentration of BPA. Whereas, the CV experiment was performed in the presence of N_2 purged 0.05 M PBS (pH 7) at a scan rate of 50 mVs^{-1} . Additionally, the concentration of BPA is varied from 0 to $300 \mu\text{M}$. The resultant CV curves is shown in Figure 5A, which clearly indicates that the oxidation current was gradually increased with increasing the concentration of BPA. The corresponding linear curve for the variation of concentration of BPA vs. oxidation peak current was shown in Figure 5B with a linear regression equation of $I_{\text{pa}} = 0.338 - 2.003$ and a correlation coefficient of $R^2 = 0.960$. It implies the high electrocatalytic activity of $\text{YMoO}_4/\text{f-CNF}/\text{GCE}$ towards the detection of BPA.

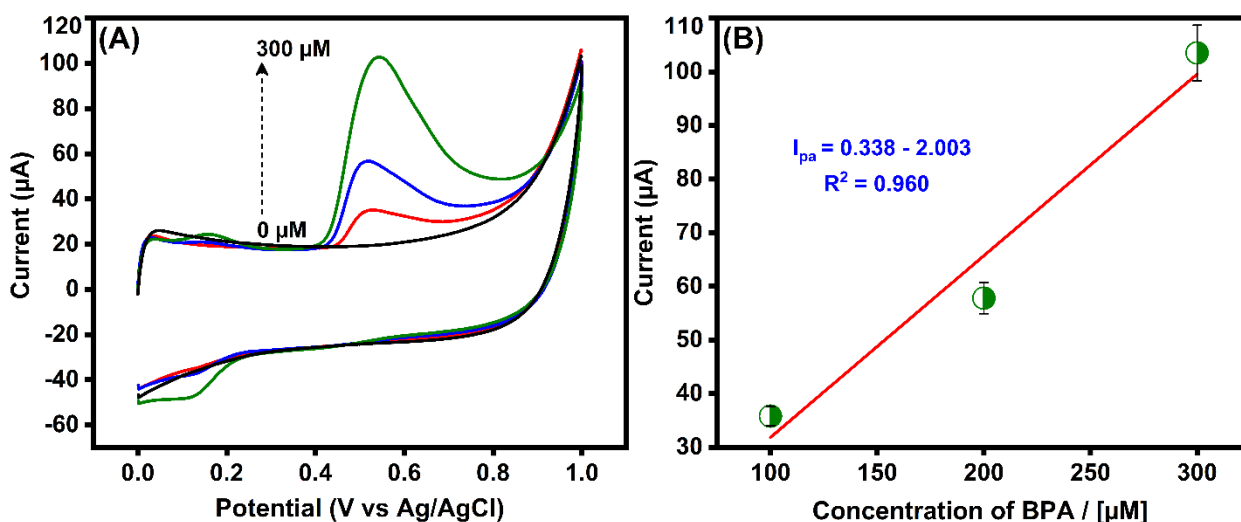


Figure 5. (A) CVs for BPA in the concentration range of 0 – 300 μM at the $\text{YMoO}_4/\text{f-CNF}/\text{GCE}$. (B) Linear calibration plot of anodic peak current vs. concentration of BPA in the range mentioned in (A).

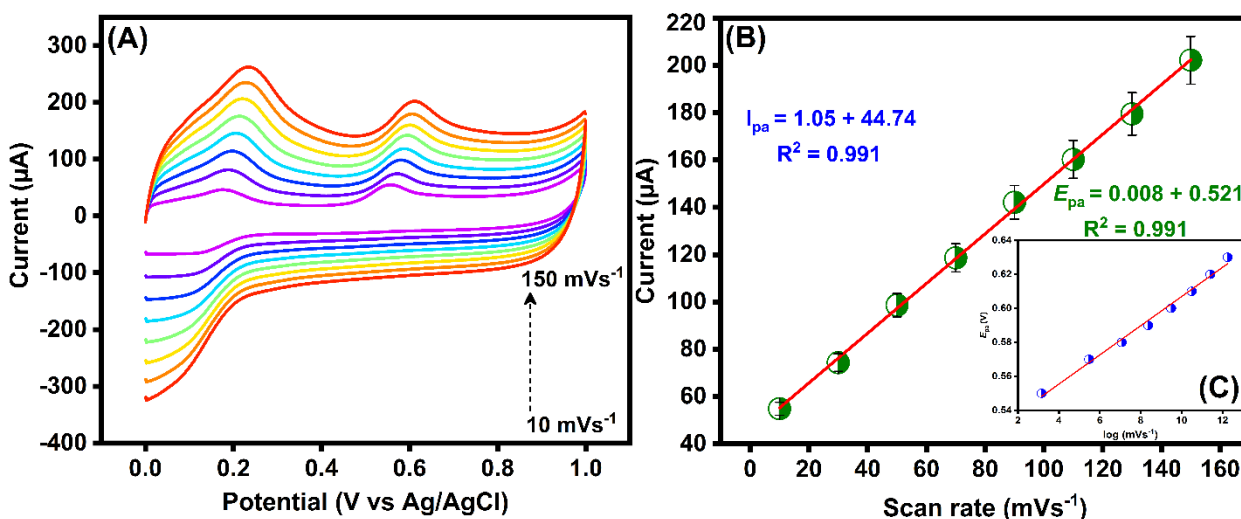


Figure 6. (A) CVs of 300 μM BPA on the $\text{YMoO}_4/\text{f-CNF}/\text{GCE}$ at different scan rates (10 - 150 mVs^{-1}). (B) The linear plot between the oxidation peak current and the scan rate. (C) The relationship between the peak potential and the logarithm of scan rate.

3.4. Effect of scan rate on the modified electrode

The electrochemical properties of modified electrode depends on variation with the scan rate. Therefore, the influence of scan rate on $\text{YMoO}_4/\text{f-CNF}/\text{GCE}$ was studied by using CV analysis. For CV analysis, the experiment was performed in presence of N_2 purged 0.05 M PBS (pH 7) by varying scan rate from 10 to 150 mVs^{-1} and it shown in Figure 6A. It can be clearly seen that the oxidation peak current of BPA was gradually increased with increasing the scan rate from lower to higher (10 – 150 mVs^{-1}). The corresponding calibration plot for oxidation peak current vs. scan rate and is shown in Figure 6B with a linear regression equation of $I_{pa} = 1.05 + 44.74$ and a correlation coefficient of $R^2 = 0.991$,

respectively. From the Figure 6C (Insert Figure 6B), the linear plot was obtained between oxidation peak potential (E_{pa}) vs. logarithm of scan rate with a linear regression equation of $I_{pa} = 0.008 + 0.521$ and a correlation coefficient of $R^2 = 0.991$, From the linear plot, it is clearly evidenced that the oxidation of BPA is an irreversible and typically adsorption-controlled process.

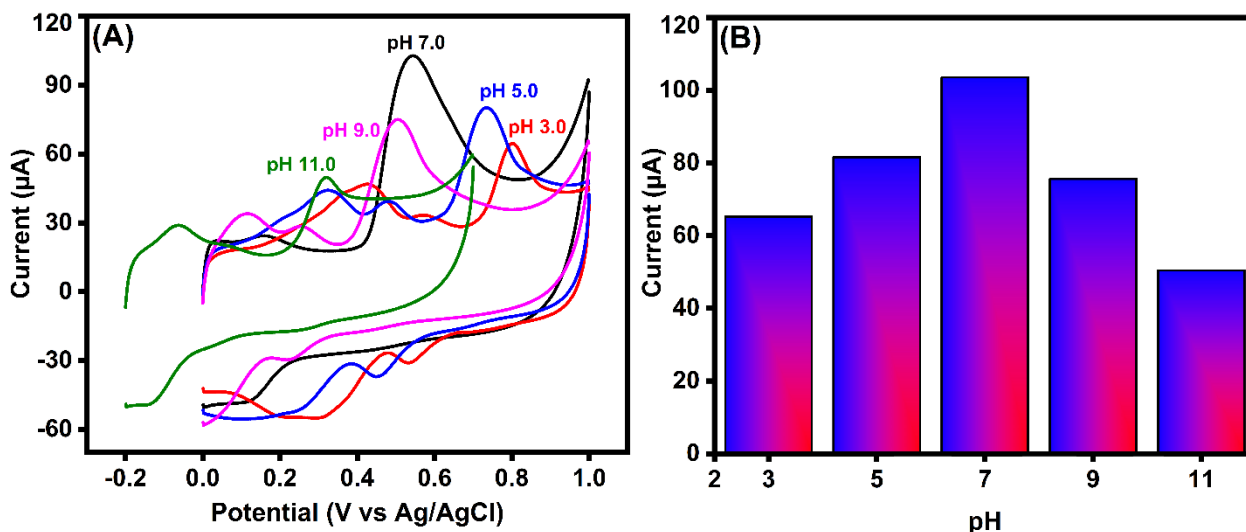


Figure 7. (A) CVs of 300 μM BPA on the $\text{YMoO}_4/\text{f-CNF}/\text{GCE}$ at different pH (3.0 – 11.0). (B) The bar diagram for the oxidation peak current and pH.

3.5. Effect of pH on modified electrode

The pH of the supporting electrolyte is another important parameter for the investigation of electrochemical reaction of $\text{YMoO}_4/\text{f-CNF}/\text{GCE}$. Thus, the effect of different pH (3.0 – 11.0) at $\text{YMoO}_4/\text{f-CNF}/\text{GCE}$ for the detection of BPA was studied by using CV. The CV curve in Figure 7A demonstrated that the oxidation peak current of BPA increases gradually with increase in pH from 3.0 to 7.0. While, the oxidation peak current decreases from varying the pH from 7.0 to 11.0. Furthermore, the peak potential was shifted to more negative side when increasing the pH values from lower to higher. Moreover, there is a sharp oxidation peak current response was observed at pH 7 (0.05 M). The corresponding bar diagram is shown in Figure 7B. It clearly confirms that the proton is a significant participator in the oxidation of BPA at $\text{YMoO}_4/\text{f-CNF}/\text{GCE}$ and the maximum oxidation peak current was obtained at pH 7.0. Therefore, pH 7.0 is considered as a supporting electrolyte throughout electrochemical experiments for the detection of BPA.

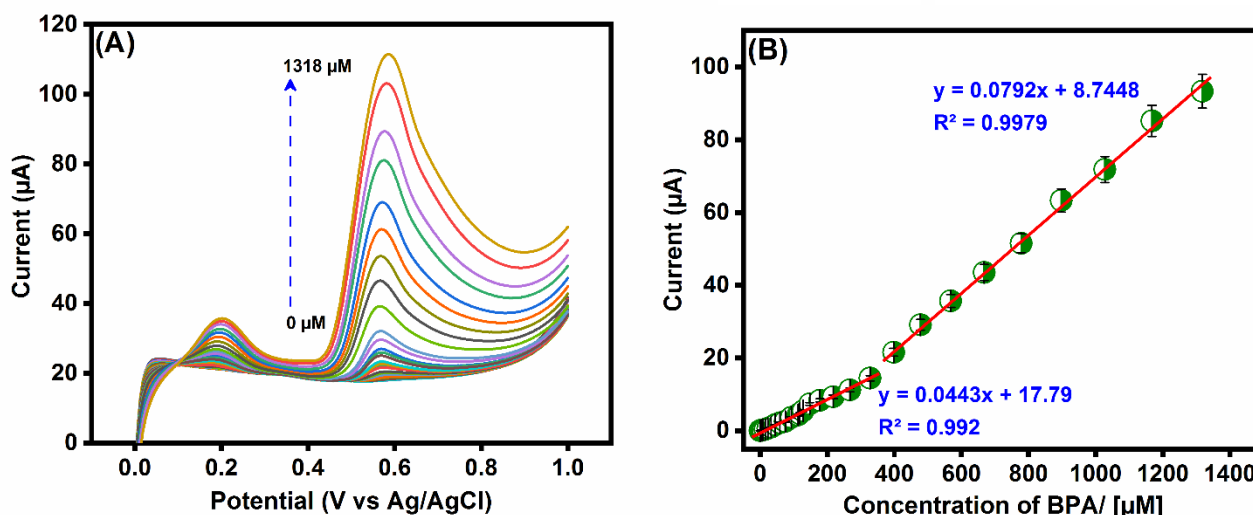


Figure 8. (A) DPV responses of electrochemical sensor (BPA) in 0.05 M PBS (pH 7.0) at the concentrations of 0.1 - 1318 μM on the $\text{YMoO}_4/\text{f-CNF}/\text{GCE}$. (B) The calibration plot between the anodic peak current and the concentration of BPA.

3.6. DPV for electrochemical detection of BPA

Table 1. Comparison of the modified electrode for electrochemical sensing of BPA.

Modified electrode	Method	Linear range (μM)	LOD (μM)	Sensitivity ($\mu\text{A } \mu\text{M}^{-1} \text{ cm}^{-2}$)	Ref
MCM-41	DPV	0.2-8.8	0.38	2.5	50
N-GS	Amperometric response	1.3-100	0.05	-	51
Mg-Al- CO_3	DPV	1.05-100	0.05	-	52
$\text{Fe}_3\text{O}_4(\text{Cs-Fe}_3\text{O}_4)$	DPV	3.0-500	0.08	-	53
BDD	DPV	0.44-5.2	0.7	-	54
PAMAM- Fe_3O_4	Amperometric response	3.07-100	0.05	-	55
$\text{YMoO}_4/\text{f-CNF}$	DPV	0.1 - 1318	0.01	0.9	This work

Differential pulse voltammetry was used to investigate the electrocatalytic activity of $\text{YMoO}_4/\text{f-CNF}/\text{GCE}$ towards electrochemical oxidation of BPA. DPV experiment was performed in presence of N_2 saturated 0.05 M PBS (pH 7.0) with varying concentration from 0.1 to 1318 μM . From the Figure 8A, it can be clearly seen that the oxidation peak current was linearly increased with increasing the concentration of BPA from lower to higher concentration. Furthermore, the linear relationship (Calibration plot) between resultant of oxidation peak current vs. concentration of BPA is clearly demonstrated in Figure 8B. The corresponding linear regression equation of $I_{\text{pa}} (\mu\text{A}) = 0.0443 (\mu\text{M}) + 17.79$ and $0.0792 (\mu\text{M}) + 8.7448$ with correlation coefficients of $R^2 = 0.992$ and $R^2 = 0.9979$. Further, the

obtained slope value in linear curve was used to calculate detection limit and sensitivity of $\text{YMoO}_4/\text{f-CNF}/\text{GCE}$ sensor by following equation.

$$\text{LOD} = 3\sigma/s$$

Whereas, the 's' indicates standard deviation of the blank value and 'm' is the slope value from the linear plot. The obtained LOD and sensitivity values are estimated to be $0.01 \mu\text{M}$ and $0.9 \mu\text{A } \mu\text{M}^{-1}\text{cm}^{-2}$. Whereas, the resultant LOD and sensitivity of $\text{YMoO}_4/\text{f-CNF}/\text{GCE}$ was compared with previously reported sensors and tabulated in Table 1. It implies that the proposed $\text{YMoO}_4/\text{f-CNF}/\text{GCE}$ which exhibit excellent electrocatalytic activity towards detection of BPA.

Table 2. Detection of BPA in water sample at $\text{YMoO}_4/\text{f-CNF}/\text{GCE}$ (n = 3)

Sample	Added (μM)	Found (μM)	Recovery (%)	RSD (%)
Waste water	0	Not found	Not found	Not found
	15	15.5	103.3	1.4
	20	20.9	104.5	1.8
	30	30.8	106	2.4

3.7. Selectivity, stability and reproducibility studies

The selectivity, stability and reproducibility of the $\text{YMoO}_4/\text{f-CNF}/\text{GCE}$ was considered as important factor for the practical application. In order to study the selectivity of $\text{YMoO}_4/\text{f-CNF}/\text{GCE}$ was analyzed. whereas, the experiment was carried out in the presence of various inorganic species and biological substances and those oxidation potentials are similar to that of BPA oxidation. The choice of interfering compounds based on the two categories, which mentioned previously in reported sensor [56]. Moreover, the high current response being observed for the addition of $50 \mu\text{M}$ BPA. While the addition of 10-fold higher concentration of interfering species such as inorganic common species (Cu^{2+} , Zn^{2+} , Mg^{2+} , Fe^{3+} , Na^+ , Ca^{2+} , I^- , Br^- , NO_3^{2-} , and Cl^-) and biological compounds (ascorbic acid, uric acid, dopamine, glucose, catechol and caffeic acid) shows negligible current response. Eventhough, BPA contains similar molecular structure as that of some interfering compounds (Dopamine and catechol) which shows little positive current response with a deviation of less than 5%. Finally, we concluded that the proposed sensor exhibits higher selectivity towards the detection of BPA. Additionally, the storage stability of the proposed $\text{YMoO}_4/\text{f-CNF}/\text{GCE}$ sensor was analyzed for one week. The obtained results clearly indicates that the $\text{YMoO}_4/\text{f-CNF}/\text{GCE}$ shows appreciable storage stability with only 4.2% oxidation peak current decrement was observed after one-week storage. Moreover, the reproducibility of the $\text{YMoO}_4/\text{f-CNF}/\text{GCE}$ sensor was performed by preparing four independent modified electrodes and experiment was conducted in the presence of BPA ($50 \mu\text{M}$) in N_2 saturated 0.05 M PBS (pH 7.0) at a scan rate of 50 mVs^{-1} with a relative standard deviation (RSD) of 3.5 %. All the obtained results

evidenced that the proposed YMoO₄/f-CNF/GCE sensor exhibits excellent selectivity, stability and reproducibility towards BPA detection.

3.8 Real Sample Analysis

The detection of BPA in real samples were studied at YMoO₄/f-CNF/GCE by using DPV technique. For further analysis, waste water samples were collected from Taipei river. There is no pretreatment of sample to be required. Initially, 1 mL of sample solution was added into the 0.05 M PBS (pH 7.0) at scan rate of 0.05 mVs⁻¹. The experiment was repeated for several times. After that, recovery values were estimated by following standard addition method and its corresponding values ranging from 103.3% to 106 % and shown in Table (2). The obtained recovery values suggest that the YMoO₄/f-CNF/GCE acts as excellent electrocatalyst, which is more suitable material for the detection of BPA.

4. CONCLUSIONS

In summary, we have prepared YMoO₄ nanosheets functionalized integrated carbon nanofiber (f-CNF) by using simple ultrasonication method. Further, YMoO₄ NSs and YMoO₄/f-CNF nanocomposite was characterized by using various spectroscopic techniques such as XRD, HR-TEM, and RAMAN. From the results of spectroscopic analysis, the successful formation of YMoO₄ and YMoO₄/f-CNF nanocomposite was confirmed. Further, as-prepared YMoO₄/f-CNF composite was applied for the electrochemical detection of BPA. The electrochemical properties of YMoO₄/f-CNF composite modified electrode was investigated by using CV and DPV technique. As we expected, YMoO₄/f-CNF/GCE exhibits high electrocatalytic activity towards the detection of BPA with good detection limit (0.01 μM) and obtained with a sensitivity of (0.9 μA μM⁻¹cm⁻²). Therefore, we are successfully reported that the feasible selectivity, storage stability and reproducibility of the proposed sensor, which reveals more advantages for the excellent practicability of YMoO₄/f-CNF/GCE to determine BPA in real sample analysis.

ACKNOWLEDGEMENTS

The authors gratefully acknowledge the financial support of the National Taipei University of Technology, and National Taiwan Ocean University Joint Research Program (USTP- NTUT- NTOU-108-02).

References

1. X. Lin, P. Terry, J. Chen, J. Wu, C. Cheng, H. Cui, *Biosens. Bioelectron.*, 91 (2016) 104.
2. L.N. Vandenberg, R. Hauser, M. Marcus, N. Olea, W. V. Welshons, *Reprod. Toxicol.*, 24 (2007) 139.
3. S.N. Loganathan, K. Kannan, *Arch. Environ. Contam. Toxicol.*, 61 (2011) 68.
4. C. Huang, Y. Wu, J. Chen, Z. Han, J. Wang, H. Pan, M. Du, *Electroanalysis*, 24 (2012) 1416.
5. B.Y. Su, H.L. Shao, N. Li, X.M. Chen, Z.X. Cai, X. Chen, *Talanta*, 166 (2017) 126.
6. A.M. Calafat, J. Weuve, X. Ye, L.T. Jia, H. Hu, S. Ringer, K. Huttner, R. Hauser, *Environ. Health Perspect.*, 117 (2009) 639.
7. N. Zehani, P. Fortgang, M.S. Lachgar, A. Baraket, M. Arab, S. V. Dzyadevych, R. Kherrat, N.

- Jaffrezic-Renault, *Biosens. Bioelectron*, 77 (2016) 1222.
8. Pan, Bo, D. Lin, H. Mashayekhi, B. Xing, *Environmental science & technology*, 42 (2008) 5480.
 9. N. Zehani, P. Fortgang, M. S. Lachgar, *Biosens. Bioelectron*, 74 (2015) 830.
 10. G Delbès, C Levacher, R. Habert, *Reproduction*, 132 (2006) 527.
 11. H. Hamid, C. Eskicioglu, *Water Res*, 46(2012), 5813.
 12. C. Thompson, T. Berl, A. Tejedor, G. Johannsson, *Res. Clin. Endocrinol. Metab*, 26 (2012) S7.
 13. R.R. Gerona, T.J. Woodruff, C.A. Dickenson, J. Pan, J.M. Schwartz, S. Sen, M.W. Friesen, V.Y. Fujimoto, P.A. *Environ. Sci. Technol*, 47 (2013) 12477.
 14. P. Giovannelli, A. Bilancio, A. Migliaccio, G. Galasso, G. Cernerla, G. Castoria, M. Di Donato, *Mol. Cell. Endocrinol*, 457 (2017) 35.
 15. Q. Wang, Y. Wang, S. Liu, L. Wang, F. Gao, F. Gao, W. Sun, *Thin Solid Films*, 520 (2012) 4459.
 16. C. Erler, J. Novak, *J. Pediatr. Nurs*, 25 (2010) 400.
 17. T. Colborn, S. Frederick, *Environ. Heal*, 101 (2012) 378.
 18. R.H. Waring, R.M. Harris, *Mol. Cell. Endocrinol*, 244 (2005) 2.
 19. R.T. Zoeller, R. Bansal, C. Parris, *Endocrinology*, 146 (2005) 607.
 20. A. Ballesteros-Gómez, S. Rubio, D. Pérez-Bendito, *J. Chromatogr. A*, 1216 (2009) 449.
 21. D.L. Villeneuve, N. Garcia-Reyero, B.L. Escalon, K.M. Jensen, J.E. Cavallin, E.A. Makynen, E.J. Durhan, M.D. Kahl, L.M. Thomas, E.J. Perkins, G.T. Ankley, *Environ. Sci. Technol*, 46 (2012) 51.
 22. J.H. Kang, D. Aasi, Y. Katayama, *Crit. Rev. Toxicol*, 37 (2007) 607.
 23. C. A. Staples, P. B. Dome, G. M. Klecka, S. T. Oblock, L. R. Harris, *Chemosphere*, 36 (1998) 2149.
 24. B. Carlos, P. Cinta, J.B. Donald, *Ecotoxicology*, 13 (2004) 511.
 25. S.J. Brennan, C.A. Brougham, J.J. Roche, A.M. Fogarty, *Chemosphere*, 64 (2006) 49.
 26. X. Wang, H. Zeng, L. Zhao, J.M. Lin, *Anal. Chim. Acta*, 556 (2006) 313.
 27. M. Amjadi, J.L. Manzoori, T. Hallaj, *J. Lumin*, 158 (2015) 160.
 28. L. sheng Hu, C.C. Fong, L. Zou, W.L. Wong, K.Y. Wong, R.S.S. Wu, M. Yang, *Biosens. Bioelectron*, 53 (2014) 406.
 29. A.O. Cheek, V.W. King, J.R. Burse, D.L. Borton, C. V. Sullivan, *Comp. Biochem. Physiol. - C Toxicol. Pharmacol*, 137 (2004) 249.
 30. X. Zhang, D. Zhu, C. Huang, Y. Sun, Y.I. Lee, *Microchem. J*, 121 (2015) 1.
 31. A.O. Cheek, V.W. King, J.R. Burse, D.L. Borton, C.V. Sullivan, *Biochem. Physiol. C*, 137 (2004) 249.
 32. P. Sundaresan, R. Karthik, S.M. Chen, J.V. Kumar, V. Muthuraj, E.R. Nagarajan, *Ultrasonics sonochemistry*, (2018).
 33. R. Karthik, J. Vinoth Kumar, S.M. Chen, P. Sundaresan, B. Mutharani, Y. Chi Chen, V. Muthuraj, *Ultrason. Sonochem*, 48 (2018) 473.
 34. R. Karthik, J. VinothKumar, S. M. Chen, T. Kokulnathan, T. WeiChen, S. Sakthinatha, T. WeiChiu, *Sensors & Actuators: B. Chemical*, 270 (2018) 353.
 35. A. Shameem, P. Devendran, V. Siva, R. Packiaraj, N. Nallamuthu, S. Asath Bahadur, *J. Mater. Sci. Mater. Electron*, 30 (2019) 3305.
 36. B. Saravanakumar, S. P. Ramachandran, G. Ravi, V. Ganesh, A. Sakunthala, R. Yuvakkumar, *Applied Physics A*, 6 (2019) 125.
 37. X. Yu, B. Lu, Z. Xu, *Adv. Mater*, 26 (2014) 1044.
 38. C. Yuan, J. Li, L. Hou, X. Zhang, L. Shen, X.W. Lou, *Adv. Funct. Mater*, 22 (2012) 4592.
 39. Y. Ding, Y. Wan, Y.L. Min, W. Zhang, S.H. Yu, *Inor. Chem*, 47 (2008) 7813.
 40. B. J. Reddy, P. Vickraman, A. S. Justin, *Phys. Status Solidi A*, 1800595 (2018) 1.
 41. L. Zhang, S. Zheng, L. Wang, H. Tang, H. Xue, G. Wang, H. Pang, *Small*, 13 (2017) 1.
 42. T. W. Chen, J. V. Kumar, S. M. Chen, B. Mutharani, R. Karthik, E.R.Nagarajan, V. Muthuraj, *Chemical Engineering Journal*, 359 (2019) 1472.
 43. Li, Congming, Yanli Zhou, Xu Zhu, Baoxian Ye, and Maotian Xu. *International Journal of Electrochemical Science* 13, (2018) 4855.

44. S. Roy, N. Soin, R. Bajpai, D. S. Misra, A. James, McLaughlin, S. S. Roy, *J. Mater. Chem*, 21(2011) 14725.
45. A. J. S. Ahammad, J. Lee Md. A. Rahman, *Sensors*, 9 (2009) 2289.
46. Y. Yao, H. Wu, J. Ping, *Food Chem*, 274 (2019) 8.
47. M. Sakthivel, S. Ramaraj, S.M. Chen, B. Dinesh, H.V. Ramasamy, Y.S. Lee, *Anal. Chim. Acta*, 1006 (2018) 22.
48. J. Huang, Y. Liu, T. You, *Anal. Method.*, 2 (2010) 202.
49. Y. Li, X. Huang, L. Zeng, R. Li1, H. Tian, X. Fu, Y. Wang, W. Zhong, *J Mater Sci*, 54 (2019) 1036.
50. F. Wang, J. Yang, K. Wu, 638 (2009). 23.
51. F. Haixia, Y. Li, D. Wu, H. Ma, K. Mao, D. Fan, B. Du, H. Li, Q. Wei, *Analytica chimica acta*, 711 (2012) 24.
52. Y. Huanshun, L. Cui, S. Ai, H. Fan, L. Zhu, *Electrochimica Acta*, 55 (2010) 603.
53. C.Yu, L. Gou, X. Zhou, N. Bao, H. Gu, *Electrochimica Acta*, 56 (2011) 9056.
54. P. F. Gabriel, S. L. Andrade, R. C. Rocha-Filho, N. Bocchi, R. Sonia, Biaggio, *Electrochimica Acta*, 82 (2012) 3.
55. Y. Huanshun, L. Cui, Q. Chen, W. Shi, S. Ai, L. Zhu, L. Lu. *Food Chemistry*, 3 (2011) 1097.
56. R. Sukanya, M. Sakthivel, S.M. Chen, T. W. Chen, *Sensors and Actuators B*, 269 (2018) 354.

© 2019 The Authors. Published by ESG (www.electrochemsci.org). This article is an open access article distributed under the terms and conditions of the Creative Commons Attribution license (<http://creativecommons.org/licenses/by/4.0/>).